

# Synthesis and characterization of mesoporous TiO<sub>2</sub> nanostructured films prepared by a modified sol–gel method for application in dye solar cells

E.C. Muniz<sup>a</sup>, M.S. Góes<sup>a,\*</sup>, J.J. Silva<sup>a</sup>, J.A. Varela<sup>a</sup>, E. Joanni<sup>b</sup>, R. Parra<sup>c</sup>, P.R. Bueno<sup>a</sup>

<sup>a</sup>Departamento de Físico-Química, Instituto de Química, UNESP, R. Francisco Degni s/n, CEP.: 14800-900, Araraquara, SP, Brazil

<sup>b</sup>Centro de Tecnologia da Informação Renato Archer, Rodovia Dom Pedro I (SP - 65) Km 143,6, CEP.: 13069-901, Campinas, SP, Brazil

<sup>c</sup>Instituto de Investigaciones en Ciencia y Tecnología de Materiales (INTEMA), CONICET-UNMDP, J.B. Justo 4302, B7608FDQ Mar del Plata, Argentina

Received 6 September 2010; received in revised form 23 September 2010; accepted 7 November 2010

Available online 2 December 2010

## Abstract

Anatase TiO<sub>2</sub> colloidal dispersions were obtained by hydrothermal synthesis at 200 °C from titanium isopropoxide gels modified with acetic acid in the presence of a non-ionic surfactant. Absolute ethanol, anhydrous terpineol and ethyl cellulose were added to this anatase dispersion resulting in a 23 wt% TiO<sub>2</sub> paste. Mesoporous films for application as working electrodes in dye-sensitized solar cells were prepared by the screen-printing method, yielding reproducible films with thicknesses about 10 μm and desired porosity levels in a single printing operation. An average energy conversion efficiency of 5.2%, and a fill factor of 0.66 were achieved with anatase particle sizes ranging between 15 and 20 nm. The reproducibility of the results was confirmed by electrochemical impedance spectroscopy analysis.

© 2010 Elsevier Ltd and Techna Group S.r.l. All rights reserved.

**Keywords:** Nanoparticle TiO<sub>2</sub>; Sol–gel; Hydrothermal synthesis; DSC

## 1. Introduction

Among semiconducting oxides, the TiO<sub>2</sub> has been the subject of a great deal of research in virtue of its outstanding physicochemical properties and the increasing demand for functional devices with enhanced properties [1–6]. Current interest is focused on the use of TiO<sub>2</sub> nanoparticles for the development of dye-sensitized solar cells (DSCs), which have attracted much attention as a viable alternative for solar energy conversion [7]. The physicochemical properties of TiO<sub>2</sub> are significantly dependent on the crystalline phase (anatase, rutile or brookite), but anatase has proven to be superior in solar energy conversion and catalytic applications.

In fact, nanostructured anatase TiO<sub>2</sub> electrodes are believed to be essential for achieving high conversion efficiencies and good long-term stability in DSCs [8]. Although there is no generally accepted explanation, this fact is commonly attributed to the structure and chemical composition of the TiO<sub>2</sub>-surface in this particular phase [9,10]. Furthermore, the

control of film thickness and area are very important points in order to obtain reproducible device performances. The development of DSCs and photocatalysis are only two of the many possible environmental applications of TiO<sub>2</sub> [11–15]. It is known that the synthesis method of the paste affects the efficiency of solar cells. In fact, the influence of the experimental parameters relevant to the synthesis of anatase has been widely studied [16–27].

Recently, Huang et al. analyzed the effects of hydrothermal temperature and TiO<sub>2</sub> film thickness on the performance of DSCs. The authors measured conversion efficiencies of 2.5 and 5.8% for films 5 and 10 μm thick, respectively [28]. According to this work, the synthesis at 240 °C resulted in optimal surface area, pore diameter and conversion efficiency for a 10 μm-thick film. Some authors have reported on the synthesis of mesoporous anatase by hydrothermal methods at 130 °C [29] and others showed that the increase of pH (to 5) after the hydrothermal treatment improves the performance of DSCs [30]. On the other hand, Ito et al. suggested that water-based pastes prepared by hydrolysis and hydrothermal treatment of titanium isopropoxide lead to poor reproducibility and developed a screen-printing procedure for TiO<sub>2</sub> films [31,32]. Their method is efficient and reproducible, but the

\* Corresponding author. Tel.: +55 16 33016642; fax: +55 16 33227932.

E-mail addresses: [marcgoes@iq.unesp.br](mailto:marcgoes@iq.unesp.br) (M.S. Góes),  
[rparra@fi.mdp.edu.ar](mailto:rparra@fi.mdp.edu.ar) (R. Parra).

process may involve many steps and several layers are needed in order to obtain considerable thicknesses. Other authors also reported on the sol–gel synthesis of titania colloids followed by hydrothermal treatments at 150–250 °C in a strong acidic media [33] or using laurylamine hydrochloride, metal alkoxide and acetylacetone [34]. A different route for screen-printing titania pastes proposed by Tsoukleris et al. led to efficiencies between 0.38 and 1.87%, showing that this procedure still needed optimization [35]. Alternatively, Kuo and Lu proposed the synthesis of TiO<sub>2</sub> inverse opal films using polystyrene spheres (100 nm) as templating agents, which increase the complexity and processing costs [36]. Ma et al. demonstrated that PEG 20000 can be used as the binder and pore-forming agent, and ethyl cellulose can efficiently control the viscosity and rheology of the paste [37]. These are very important aspects that must be considered for the synthesis of TiO<sub>2</sub> pastes for DSC applications. Besides, recent papers reported on the synthesis of anatase fibers [38] and on the hydrothermal in situ growth of anatase nanowire films used in DSCs with considerable energy conversion efficiencies [39].

Parameters such as pore diameter, shape and particle size, good connection between TiO<sub>2</sub> particles, specific surface area and amount of defects of the anatase film are essential for applications in DSCs, because they determine the adsorption of a sufficiently large number of dye molecules (needed for highly efficient light harvesting) and mobility of the electrons through the semiconductor. Moreover, the literature suggests that TiO<sub>2</sub> films with thicknesses around 10 μm lead to the best energy conversion performance [40] and, generally, this thickness can only be achieved by the deposition of several TiO<sub>2</sub> layers. On the other hand, the geometry or architecture of the electrode needs to be optimized in order to improve the performance of the solar cell [15,28,41,42]. Different dyes and electrolytes are also being tested with the purpose of maximizing light absorption [43–45].

In this paper we propose a simple synthesis route of anatase colloidal dispersions and nanostructured films deposited by the screen-printing method. The hydrothermal synthesis of TiO<sub>2</sub> was performed at 200 °C without the addition of concentrated mineral acids such as HCl, because when HCl is used, for example, as catalyst for hydrolysis, the surface of the resulting TiO<sub>2</sub> nanoparticles is inevitably contaminated with chlorine ions. In this study, titanium dioxide mesoporous films with reproducible thicknesses (~10 μm) appropriate for DSC anodes were prepared by screen-printing in a single step. A series of films was prepared and tested as working electrodes in DSCs for which morphological and electrical characterizations were carried out.

## 2. Experimental details

### 2.1. Synthesis of the TiO<sub>2</sub> paste

Analytical grade reagents were used as supplied, without further purification. Titanium isopropoxide (TIP, 97%, Aldrich) was added at room temperature to a solution of anhydrous acetic acid (HAc, Merck) and a non-ionic surfactant (NIS,

Triton X-100, Aldrich) in 2-propanol (Pr<sup>i</sup>OH, Qhemis). With the purpose of slowing down condensation reactions and immediate gelation or precipitation after water addition, TIP was modified with acetic acid in a 1:1 TIP:HAc molar ratio [46,47]. The surfactant was added in an approximate 100:1 TIP:NIS molar ratio. After 60 min a solution of water in Pr<sup>i</sup>OH was added dropwise under vigorous stirring. The amount of water incorporated into the solution was equivalent to a 1:2 TIP:H<sub>2</sub>O molar ratio. An opalescent homogeneous gel was obtained which was aged for 24 h in order to maximize the condensation of the modified precursor. Then, the gel was peptized at 80 °C and the evaporated alcohol compensated with water. Finally, the resulting dispersion was transferred into a PTFE-lined stainless steel vessel for hydrothermal treatment at 200 °C (~15 bar) for 15 h inside an electric furnace. The obtained dispersion of pH 1–2 was concentrated by evaporation. Absolute ethanol, anhydrous terpineol (Sigma–Aldrich) and ethyl cellulose (EC 5–15 mPa s, Sigma–Aldrich) were then added to the anatase dispersion. After alcohol evaporation, a 23 wt% TiO<sub>2</sub> paste was obtained. A flow diagram for the synthesis route is shown in Fig. 1.

### 2.2. Electrode preparation and DSC assembly

The synthesized oxide paste was used for the deposition of films onto conducting FTO-coated glass substrates (TCE 15 Ω cm<sup>-1</sup>) by the screen printing method. The films, having an area of 0.25 cm<sup>2</sup>, were dried at room temperature and heat-treated at 450 °C for 20 min in order to promote sintering. For dye adsorption, the films were immersed for 12 h in a 0.5 mmol L<sup>-1</sup> solution of cis-bis(isothiocyanato)bis(2,2'-bipyridyl-4,4'-dicarboxylato)-Ru(II) (N3, Solaronix) in acet-

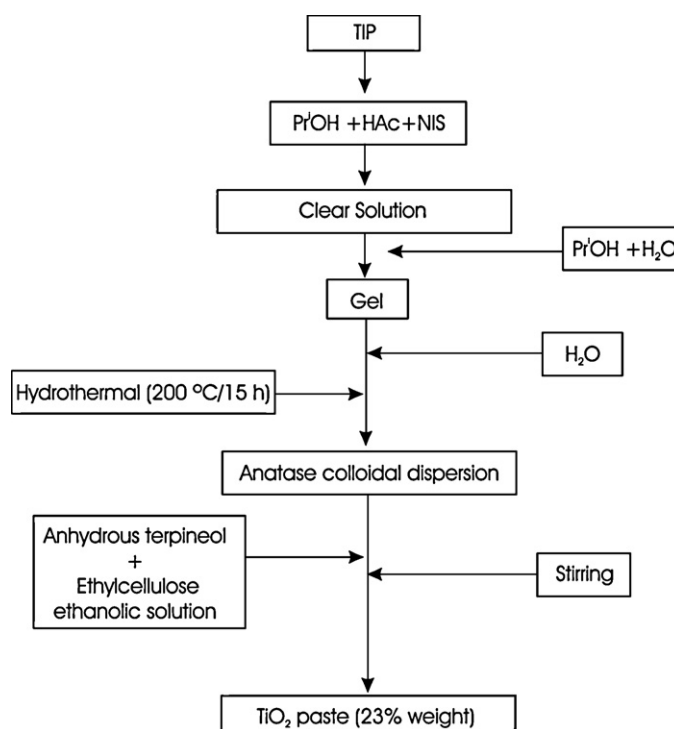


Fig. 1. Flow diagram showing the steps for synthesizing the anatase paste.

onitrile. For preparing the counter electrodes, Pt was deposited on FTO-coated glass ( $TCE\ 8\ \Omega\ cm^{-1}$ ) via thermal decomposition of  $H_2PtCl_6$  at  $450\ ^\circ C$  for 30 min. The dye-covered  $TiO_2$  electrode and Pt counter electrode were assembled into a sandwich-type cell and sealed with a  $50\ \mu m$  thick thermoplastic gasket made of Surlyn 1702. The electrolyte (Iodolyte AN-50, Solaronix) was dripped between the FTO/ $TiO_2$ /dye working electrode and the Pt-coated FTO-glass counter-electrode.

### 2.3. Characterization

Thermogravimetric and differential thermal analyses (TG/DTA) of the paste were performed using Shimadzu TG50 and DT50 equipments, respectively, under synthetic air flow (50 ml/min) with heating rates of  $10\ ^\circ C/min$ . The colloidal dispersion was heat-treated at  $450\ ^\circ C$  with heating and cooling rates of  $2\ ^\circ C/min$  in order to characterize the resulting powder. X-ray diffraction (XRD) patterns were collected using a Rigaku RINT2000 diffractometer ( $42\ kV \times 120\ mA$ ) with  $Cu\ K\alpha$  radiation ( $\lambda_{K\alpha 1} = 1.5405\ \text{\AA}$ ,  $\lambda_{K\alpha 2} = 1.5443\ \text{\AA}$ ,  $I_{K\alpha 1}/I_{K\alpha 2} = 0.5$ ),  $2\theta$  range between  $20^\circ$  and  $80^\circ$ , step size of  $0.02^\circ$  ( $2\theta$ ), 0.3 s per step, divergence slit = 0.5 mm, and receiving slit = 0.3 mm. For high-resolution transmission electron microscopy (HRTEM, Philips CM200), the powder was dispersed in ethanol in an ultrasonic bath and deposited, by dipping, onto carbon-coated copper grids. The specific surface area (BET) of the powder was determined with a Micromeritics ASAP2010 instrument. The diffuse reflectance was recorded in a Konika Minolta, CM-2500d spectrometer colorimeter in the 360–740 nm range.

The morphology of the films was assessed by field-emission scanning electron microscopy (JEOL JSM 6700F). Film thicknesses and surface profiles were measured with a Taylor Hobson Frontoy Lorsurf 50 profilometer. For the electrical characterization of the DSCs, characteristic parameters were obtained by illuminating the samples with an AM 1.5 solar simulator (SolarLight XPS400) at  $100\ mW\ cm^{-2}$ . The current–voltage ( $j$ – $V$ ) data were acquired with an Autolab PGSTAT-30 potentiostat–galvanostat. Electrochemical impedance spectroscopy (EIS) was carried out by using a Solartron impedance meter (model SI 1287). The impedance spectra from the sealed DSCs were measured in a two-electrode configuration in the dark using a bias voltage of  $-0.8\ V$  with a 20 mV AC perturbation over a frequency range of 10 mHz to 1 MHz.

## 3. Results and discussion

### 3.1. Characterization of the $TiO_2$ paste

The thermogravimetric (TGA) and differential thermal analysis (DTA) of the  $TiO_2$  paste are shown in Fig. 2. The TGA curve shows a 20% weight loss, associated to the volatilization and decomposition of organic species such as ethanol, ethyl cellulose and terpineol and residues of acetic acid and isopropyl acetate. This significant weight loss in the  $160$ – $410\ ^\circ C$  range is attributed to combustion of the organic compounds, as observed in the DTA curve (exothermic peak at  $280\ ^\circ C$ ). It is worth noting the absence of an exothermic peak that could be

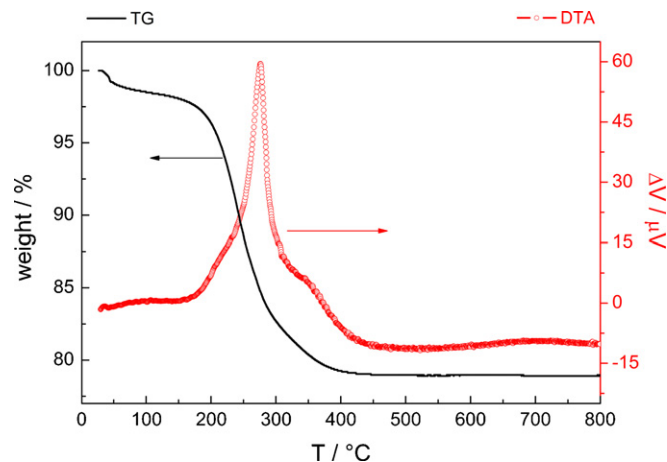


Fig. 2. Thermal behavior of the  $TiO_2$  anatase paste.

associated to the crystallization of  $TiO_2$ , confirming that the material has crystallized into anatase  $TiO_2$  during the hydrothermal treatment. The signal due to anatase formation could be observed as a narrow peak near  $400\ ^\circ C$  in the DTA of the gel obtained before the hydrothermal treatment (see supplementary information). Based on these results,  $450\ ^\circ C$  was the selected temperature for film sintering.

The XRD pattern of the colloidal dispersion dried at  $100\ ^\circ C$  is shown in Fig. 3(a). It can be observed that the precursor has crystallized into the anatase phase during the hydrothermal treatment and that the reflections corresponding to the other  $TiO_2$  polymorphs are absent. The diffractogram in Fig. 3(b) reveals that the phase is preserved after a thermal treatment at  $450\ ^\circ C$ , as expected, because the phase transition from anatase to rutile takes place near  $650\ ^\circ C$ . The Raman spectrum (see supplementary information) confirmed the sole presence of anatase in the heat-treated powder.

Fig. 4(a) shows a bright-field TEM image of the powder obtained after the thermal treatment of the synthesized paste at  $450\ ^\circ C$ . It is a well dispersed powder with an average particle size between 15 and 20 nm. The HR-TEM image (Fig. 4(b))

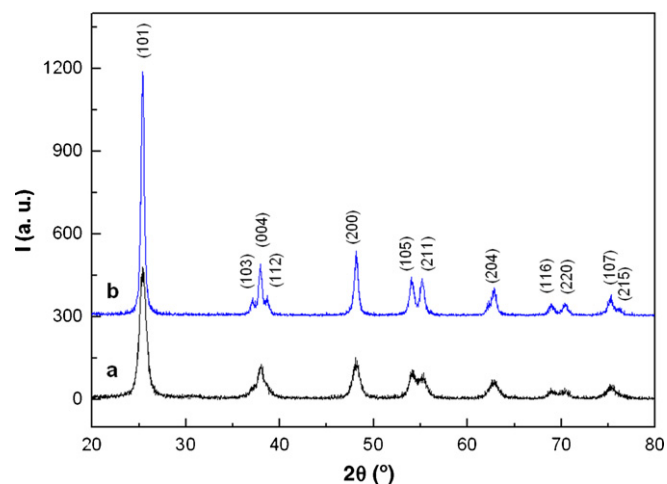


Fig. 3. XRD patterns of: (a) the as-synthesized colloidal dispersion and (b) the same sample after heat-treatment at  $450\ ^\circ C$ .

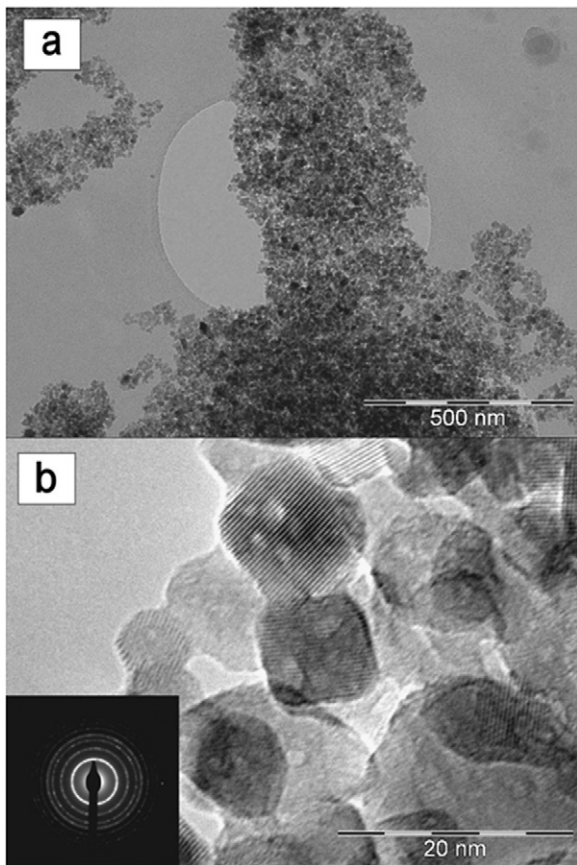


Fig. 4. (a) Low and (b) high magnification TEM images of the anatase powder obtained after treating the colloidal dispersion at 450 °C. The inset in (b) shows the SAED pattern typical of polycrystalline anatase TiO<sub>2</sub>.

reveals the high degree of crystallinity of the titanium oxide nanoparticles. The selected area electron diffraction (SAED) pattern, shown as an inset in Fig. 4(b), is typical for anatase.

The specific BET surface area for the powder after the 450 °C heat-treatment was 80 m<sup>2</sup>/g. This surface area is higher than the ones reported in the literature for similar heat treatments (69.9 m<sup>2</sup>/g [48] and 72 m<sup>2</sup>/g [49]) and is advantageous for the adsorption of a large amount of light-harvesting dye and, therefore, for light conversion efficiency improvement.

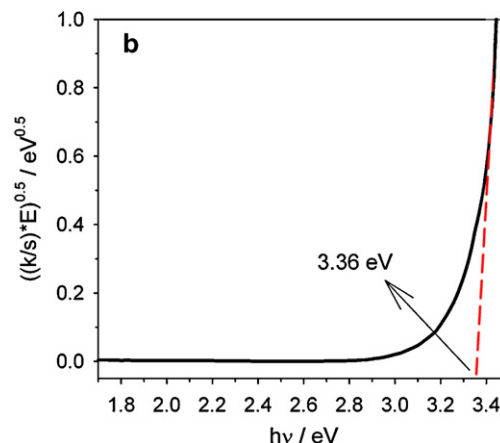
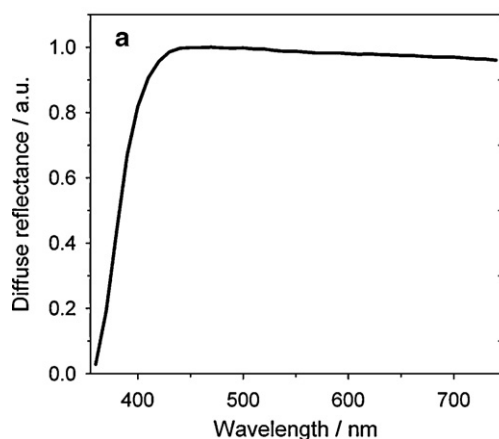


Fig. 5. (a) Diffuse reflectance curve of the TiO<sub>2</sub> powder heat-treated at 450 °C and (b) determination of optical band-gap by Tauc linearization.

Fig. 5(a) shows the UV–vis reflectance of the powder treated at 450 °C. The TiO<sub>2</sub> band-gap energy was determined by the Kubelka–Munk model and the Tauc linearization (Fig. 5(b)). The optical band-gap value determined (3.36 eV) was higher than the ones usually found in the literature (around 3.2 eV) [50]. This difference may be attributed to the small particle size of the powder characterized in this work. Once more, it can be said that the synthesized material is suitable for solar-cell applications because the recombination processes are decreased in semiconductors with wider band gaps.

### 3.2. Microstructural characterization of TiO<sub>2</sub> films

The 23 wt% paste was used for the deposition of films onto FTO-coated glass by the screen printing method. Fig. 6 shows the surface profile of 3 TiO<sub>2</sub> films heat-treated at 450 °C as registered by profilometry. Notice the uniformity in film thickness derived from the characteristics of the synthesized paste and the reproducibility of the method employed for film deposition.

Normally, in order to achieve high energy conversion, thicknesses above 10 μm are only attained after the deposition of several layers. However, by means of the procedure described here, 10 μm-thick films with a highly reproducible profile are achieved in a single operation.

As shown in the FE-SEM images (Fig. 7), the films are highly homogeneous and porous, with a very narrow size distribution of partially sintered nanoparticles of almost 20 nm. These microstructural characteristics (porosity and particle size) determine the degree of dye adsorption.

### 3.3. Electrical characterization of DSCs

The photocurrent–voltage characteristics of three DSCs tested at room temperature are shown in Fig. 8 and Table 1 shows the main parameters derived from these curves.

The samples tested showed comparable curves and performance parameters. The short circuit current density ranges between 10.8 and 11.7 mA/cm<sup>2</sup> and the open circuit voltage ranges between 0.70 and 0.72 V, i.e., the variations are

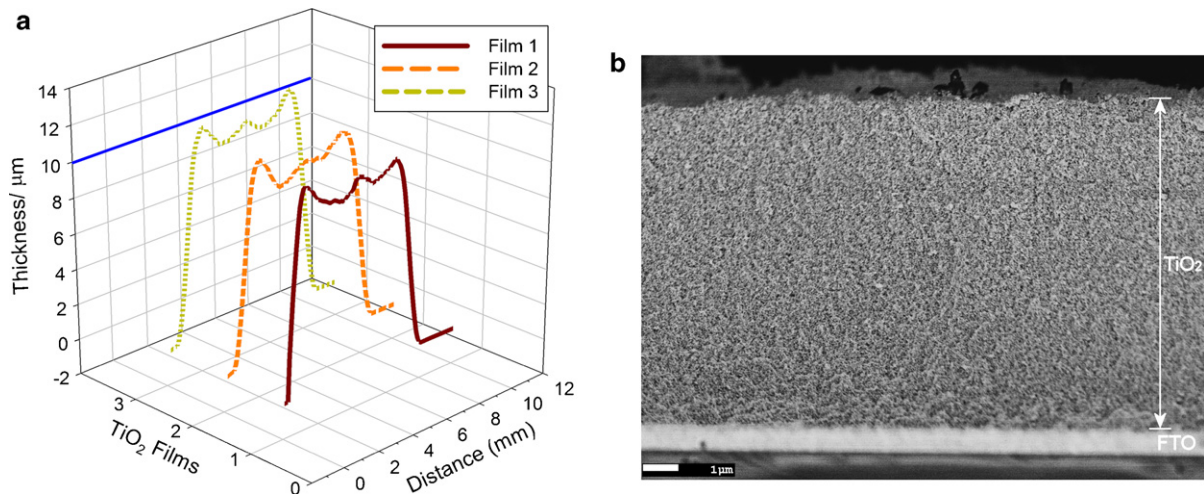


Fig. 6. (a) Profilometry curves of three TiO<sub>2</sub> films after heat treatment and (b) FE-SEM image of thickness anatase film.

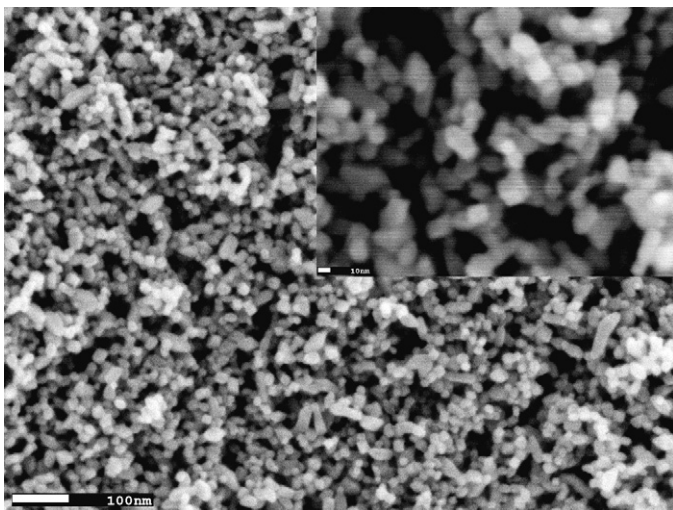


Fig. 7. FE-SEM image of a 10 μm-thick anatase film heat-treated at 450 °C. The inset shows partial sintering between particles.

within 3%. An average fill factor (FF) of 0.66 and overall conversion efficiencies ( $\eta$ ) between 4.9 and 5.2% were measured for the three anatase films used as anodes for DSCs. The small differences can be attributed to the nature of the assembly procedure. Nonetheless, these results show the reproducibility achieved in anode preparation and cell assembly. For instance, the 3 cells showed almost the same conversion efficiency. The important point is that the films were made in a single step. Besides, the cell stability is another relevant factor for DSC application, which strongly depends, among other factors, on dye and electrolyte coupling [51–53].

In order to compare qualitatively the electron transport properties in TiO<sub>2</sub> film electrodes, EIS measurements were carried out on samples with almost the same efficiency values (samples T2 and T3). Figs. 9 and 10 show the Nyquist plots measured in dark at  $-0.8$  V and  $-0.7$  V bias, respectively.

The Nyquist plots exhibit three semicircles including a large semicircle at intermediate frequencies and two small arcs in the

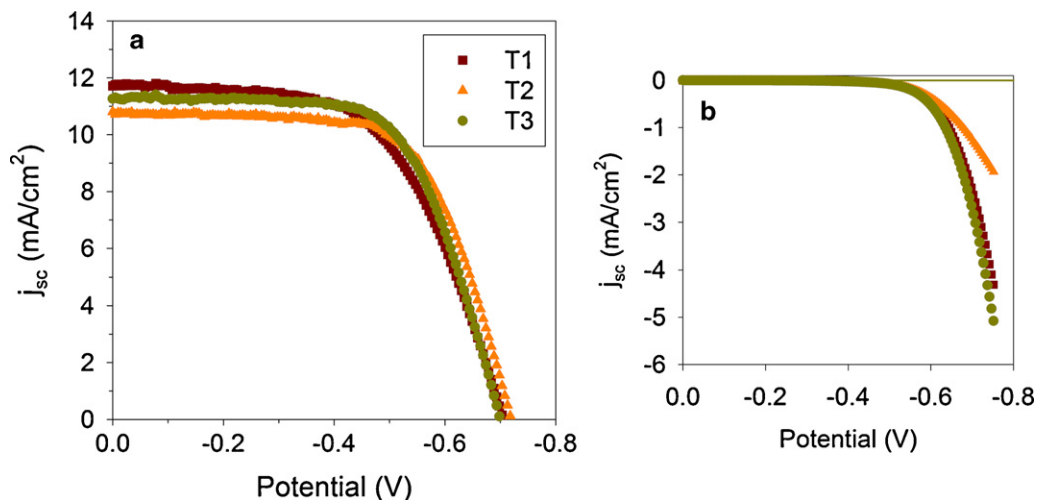


Fig. 8. Photocurrent–voltage characteristics of DSSCs based on 10 μm-thick anatase anodes.

Table 1

DSSC performance parameters: open-circuit voltage ( $V_{oc}$ ), short-circuit current density ( $j_{sc}$ ), fill factor (FF) and conversion efficiency ( $\eta$ ).

Films	$V_{oc}$ (V)	$j_{sc}$ (mA/cm <sup>2</sup> )	FF	$\eta$ (%)
T1 (■)	0.71	11.7	0.59	4.9
T2 (▲)	0.72	10.8	0.66	5.1
T3 (●)	0.70	11.3	0.65	5.2

low and high frequency regions. Basically, these two small arcs correspond to the parallel combination of the charge-transfer resistance and the double-layer capacitance at the counter electrode (Pt-FTO), and to the diffusion impedance in the electrolyte, respectively. The main arc at intermediate frequencies can be associated with the contribution of the dye-sensitized nanocrystalline TiO<sub>2</sub> film; more precisely, to the

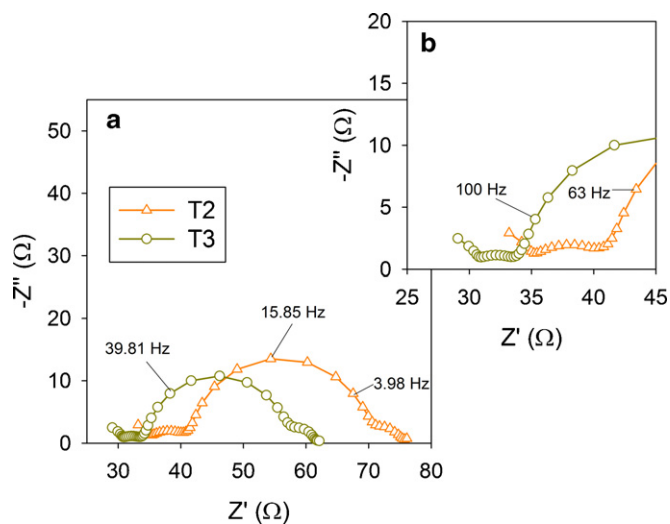


Fig. 9. Nyquist impedance diagrams of sealed DSCs based on TiO<sub>2</sub> photoelectrode (sample T2 and T3) at  $-0.80$  V forward bias. The inset shows a magnified view of the same spectra in the high frequency range.

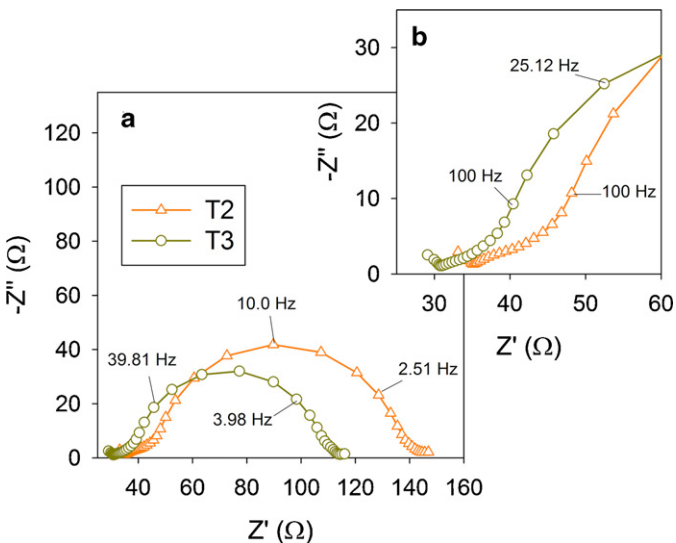


Fig. 10. Nyquist impedance diagrams of sealed DSCs based on TiO<sub>2</sub> photoelectrode (sample T2 and T3) at  $-0.70$  V forward bias. The inset shows a magnified view of the same spectra in the high frequency range.

parallel combination of the charge-transfer resistance and chemical capacitance of TiO<sub>2</sub> film [54,55]. The charge-transfer resistance is originated in the charge recombination process between electrons in TiO<sub>2</sub> films and I<sub>3</sub><sup>-</sup> in the electrolyte. Fabregat-Santiago et al. showed the influence of the different resistances over the DSCs characteristics. They showed that when the series resistance is higher, the fill factor decreases, decreasing the overall efficiency of the cell [55]. In the present case, a qualitative assessment of the impedance results reveals that the series resistance is relatively high in both samples. This fact is responsible for the low FF (Table 1). However, it is worth mentioning that a dense TiO<sub>2</sub> thin layer usually deposited onto the substrate, prior to the porous film, was not employed in this work. This dense layer has a beneficial contribution towards the light-to-electric power conversion [49,56]. The EIS results show that the cells made from our TiO<sub>2</sub> films have the same chemical kinetics.

#### 4. Conclusions

An anatase colloidal dispersion was synthesized by means of a modified sol-gel method followed by a hydrothermal treatment at 200 °C. Reproducible films (thickness around 10 μm) were prepared by screen-printing a single TiO<sub>2</sub> layer onto FTO-glass. The obtained films were porous, free of agglomerates and cracks, having particle sizes between 15 and 20 nm. A light-to-electricity conversion efficiency up to 5%, with a fill factor of 0.66, was achieved under AM1.5 simulated sunlight. The qualitative analysis by EIS shows that the cells made from the TiO<sub>2</sub> films present a similar kinetic behavior. The synthesized anatase paste showed good characteristics for application in DSCs.

#### Acknowledgements

The financial support of the research funding agencies Fundação de Amparo à Pesquisa do Estado de São Paulo (FAPESP) and Conselho Nacional de Desenvolvimento Científico e Tecnológico (CNPq) (Brazil) and CONICET (Argentina) is acknowledged.

#### Appendix A. Supplementary data

Supplementary data associated with this article can be found, in the online version, at [doi:10.1016/j.ceramint.2010.11.014](https://doi.org/10.1016/j.ceramint.2010.11.014).

#### References

- [1] C.J. Barbé, F. Arendse, P. Comte, M. Jirousek, F. Lenzmann, V. Shklover, M. Grätzel, Nanocrystalline titanium oxide electrodes for photovoltaic applications, *J. Am. Ceram. Soc.* 80 (1997) 3157–3171.
- [2] E. Traversa, M.L. Di Vona, S. Licoccia, M. Sacerdoti, M.C. Carotta, M. Gallana, G. Martinelli, Sol-gel nanosized semiconducting titania-based powders for thick-film gas sensors, *J. Sol-Gel Sci. Technol.* 19 (2000) 193–196.
- [3] G.J.D.A.A. Soler-Illia, A. Louis, C. Sanchez, Synthesis and characterization of mesostructured titania-based materials through evaporation-induced self-assembly, *Chem. Mater.* 14 (2002) 750–759.

- [4] C. Sanchez, C. Boissière, D. Grosso, C. Laberty, L. Nicole, Design, synthesis, and properties of inorganic and hybrid thin films having periodically organized nanoporosity, *Chem. Mater.* 20 (2008) 682–737.
- [5] K.H. Zuo, D.L. Jiang, J.X. Zhang, Q.L. Lin, Forming nanometer TiO<sub>2</sub> sheets by nonaqueous tape casting, *Ceram. Int.* 33 (2007) 477–481.
- [6] M.N. An'amt, S. Radiman, N.M. Huang, M.A. Yarmo, N.P. Ariyanto, H.N. Lim, M.R. Muhamad, Sol–gel hydrothermal synthesis of bismuth–TiO<sub>2</sub> nanocubes for dye-sensitized solar cell, *Ceram. Int.* 36 (2010) 2215–2220.
- [7] B. O'regan, M. Grätzel, A low-cost, high-efficiency solar cell based on dye-sensitized colloidal TiO<sub>2</sub> films, *Nature* 353 (1991) 737–740.
- [8] M.A. Green, K. Emery, D.L. King, Y. Hishikawa, W. Warta, Solar cell efficiency tables, *Prog. Photovolt. Res. Appl.* 14 (2006) 455–461.
- [9] N.G. Park, J. Van De Lagemaat, A.J. Frank, Comparison of dye-sensitized rutile- and anatase-based TiO<sub>2</sub> solar cells, *J. Phys. Chem. B* 104 (2000) 8989–8994.
- [10] J. Takahashi, H. Itoh, S. Motai, S. Shimada, Dye adsorption behavior of anatase- and rutile-type TiO<sub>2</sub> nanoparticles modified by various heat-treatments, *J. Mater. Sci.* 38 (2003) 1695–1702.
- [11] Y. Hu, H.L. Tsai, C.L. Huang, Effect of brookite phase on the anatase–rutile transition in titania nanoparticles, *J. Eur. Ceram. Soc.* 23 (2003) 691–696.
- [12] P. De Almeida, J. Van Deelen, C. Catry, H. Sneyers, T. Pataki, R. Andriessen, C. Van Roost, J.M. Kroon, Microstructure characterization of titanium dioxide nanodispersions and thin films for dye-sensitized solar cell devices, *Appl. Phys. A: Mater. Sci. Process.* 79 (2004) 1819–1828.
- [13] D. Gutiérrez-Tauste, I. Zumeta, E. Vigil, M.A. Hernández-Fenollosa, X. Domènech, J.A. Ayllón, New low-temperature preparation method of the TiO<sub>2</sub> porous photoelectrode for dye-sensitized solar cells using UV irradiation, *J. Photochem. Photobiol. A* 175 (2005) 165–171.
- [14] A.L. Castro, M.R. Nunes, A.P. Carvalho, F.M. Costa, M.H. Florêncio, Synthesis of anatase TiO<sub>2</sub> nanoparticles with high temperature stability and photocatalytic activity, *Solid State Sci.* 10 (2008) 602–606.
- [15] S. Nakade, Y. Saito, W. Kubo, T. Kitamura, Y. Wada, S. Yanagida, Influence of TiO<sub>2</sub> nanoparticle size on electron diffusion and recombination in dye-sensitized TiO<sub>2</sub> solar cells, *J. Phys. Chem. B* 107 (2003) 8607–8611.
- [16] E. Scolan, C. Sanchez, Synthesis and characterization of surface-protected nanocrystalline titania particles, *Chem. Mater.* 10 (1998) 3217–3223.
- [17] N. Steunou, F. Robert, K. Boubekeur, F. Ribot, C. Sanchez, Synthesis through an in situ esterification process and characterization of oxo isopropoxo titanium clusters, *Inorg. Chim. Acta* 279 (1998) 144–151.
- [18] P.A. Venz, R.L. Frost, J.T. Kloprogge, Chemical properties of modified titania hydrolysates, *J. Non-Cryst. Solids* 276 (2000) 95–112.
- [19] C. Wang, Z.X. Deng, Y. Li, The synthesis of nanocrystalline anatase and rutile titania in mixed organic media, *Inorg. Chem.* 40 (2001) 5210–5214.
- [20] U. Schubert, Chemical modification of titanium alkoxides for sol–gel processing, *J. Mater. Chem.* 15 (2005) 3701–3715.
- [21] F. Bosc, P. Lacroix-Desmazes, A. Ayrat, TiO<sub>2</sub> anatase-based membranes with hierarchical porosity and photocatalytic properties, *J. Colloid Interface Sci.* 304 (2006) 545–548.
- [22] M.C. Fuertes, G.J.A.A. Soler-Illia, Processing of macroporous titania thin films: from multiscale functional porosity to nanocrystalline macroporous TiO<sub>2</sub>, *Chem. Mater.* 18 (2006) 2109–2117.
- [23] S. Cassaignon, M. Koelsch, J.-P. Jolivet, From TiCl<sub>3</sub> to TiO<sub>2</sub> nanoparticles (anatase, brookite and rutile): thermohydrolysis and oxidation in aqueous medium, *J. Phys. Chem. Solids* 68 (2007) 695–700.
- [24] N.R. Neale, A.J. Frank, Size and shape control of nanocrystallites in mesoporous TiO<sub>2</sub> films, *J. Mater. Chem.* 17 (2007) 3216–3221.
- [25] W. Zhang, S. Chen, S. Yu, Y. Yin, Experimental and theoretical investigation of the pH effect on the titania phase transformation during the sol–gel process, *J. Cryst. Growth* 308 (2007) 122–129.
- [26] J.A. Chang, M. Vithal, I.C. Baek, S.I. Seok, Morphological and phase evolution of TiO<sub>2</sub> nanocrystals prepared from peroxotitanate complex aqueous solution: influence of acetic acid, *J. Solid State Chem.* 182 (2009) 749–756.
- [27] L.D. Marco, M. Manca, R. Giannuzzi, F. Malara, G. Melcarne, G. Ciccarella, I. Zama, R. Cingolani, G. Gigli, Novel preparation method of TiO<sub>2</sub>-nanorod-based photoelectrodes for dye-sensitized solar cells with improved light-harvesting efficiency, *J. Phys. Chem. C* 114 (2010) 4228–4236.
- [28] C.-Y. Huang, Y.-C. Hsu, J.-G. Chen, V. Suryanarayanan, K.-M. Lee, K.-C. Ho, The effects of hydrothermal temperature and thickness of TiO<sub>2</sub> film on the performance of a dye-sensitized solar cell, *Sol. Energy Mater. Sol. Cells* 90 (2006) 2391–2397.
- [29] S. Pavasupree, J. Jitputti, S. Ngamsinlapasathian, S. Yoshikawa, Hydrothermal synthesis, characterization, photocatalytic activity and dye-sensitized solar cell performance of mesoporous anatase TiO<sub>2</sub> nanopowders, *Mater. Res. Bull.* 43 (2008) 149–157.
- [30] T.M. Paronyan, A.M. Kechiantz, M.C. Lin, Highly active nanocrystalline TiO<sub>2</sub> photoelectrodes, *Nanotechnology* 19 (2008) 115201–119801.
- [31] S. Ito, P. Chen, P. Comte, M.K. Nazeeruddin, P. Liska, P. Péchy, M. Grätzel, Fabrication of screen-printing pastes from TiO<sub>2</sub> powders for dye-sensitized solar cells, *Prog. Photovolt. Res. Appl.* 15 (2007) 603–612.
- [32] S. Ito, T.N. Murakami, P. Comte, P. Liska, C. Grätzel, M.K. Nazeeruddin, M. Grätzel, Fabrication of thin film dye sensitized solar cells with solar to electric power conversion efficiency over 10%, *Thin Solid Films* 516 (2007) 4613–4619.
- [33] P. Wang, S.M. Zakeeruddin, P. Comte, R. Charvet, R. Humphry-Baker, M. Grätzel, Enhance the performance of dye-sensitized solar cells by co-grafting amphiphilic sensitizer and hexadecylmalonic acid on TiO<sub>2</sub> nanocrystals, *J. Phys. Chem. B* 107 (2003) 14336–14341.
- [34] S. Pavasupree, Y. Suzuki, S. Pivsa-Art, S. Yoshikawa, Preparation and characterization of mesoporous MO<sub>2</sub> (M = Ti, Ce, Zr, and Hf) nanopowders by a modified sol–gel method, *Ceram. Int.* 31 (2005) 959–963.
- [35] D.S. Tsoukleris, I.M. Arabatzis, E. Chatzivasiloglou, A.I. Kontos, V. Belessi, M.C. Bernard, P. Falaras, 2-Ethyl-1-hexanol based screen-printed titania thin films for dye-sensitized solar cells, *Sol. Energy* 79 (2005) 422–430.
- [36] C.-Y. Kuo, S.-Y. Lu, Fabrication of a multi-scale nanostructure of TiO<sub>2</sub> for application in dye-sensitized solar cells, *Nanotechnology* 19 (2008) 095101–099801.
- [37] L. Ma, M. Liu, T. Peng, K. Fan, L. Lu, K. Dai, Fabrication and properties of meso–macroporous electrodes screen-printed from mesoporous titania nanoparticles for dye-sensitized solar cells, *Mater. Chem. Phys.* 118 (2009) 477–483.
- [38] R. Sui, V. Thangadurai, C.P. Berlinguette, Simple protocol for generating TiO<sub>2</sub> nanofibers in organic media, *Chem. Mater.* 20 (2008) 7022–7030.
- [39] X. Feng, K. Shankar, O.K. Varghese, M. Paulose, T.J. Latempa, C.A. Grimes, Vertically aligned single crystal TiO<sub>2</sub> nanowire arrays grown directly on transparent conducting oxide coated glass: synthesis details and applications, *Nano Lett.* 8 (2008) 3781–3786.
- [40] M. Wei, Y. Konishi, H. Zhou, M. Yanagida, H. Sugihara, H. Arakawa, Highly efficient dye-sensitized solar cells composed of mesoporous titanium dioxide, *J. Mater. Chem.* 16 (2006) 1287–1293.
- [41] H. Al-Dmour, D.M. Taylor, J.A. Cambridge, Effect of nanocrystalline-TiO<sub>2</sub> morphology on the performance of polymer heterojunction solar cells, *J. Phys. D: Appl. Phys.* 40 (2007) 5034–5038.
- [42] E. Joanni, R. Savu, M.S. Góes, P.R. Bueno, J.N. De Freitas, A.F. Nogueira, E. Longo, J.A. Varela, Dye-sensitized solar cell architecture based on indium–tin oxide nanowires coated with titanium dioxide, *Scripta Mater.* 57 (2007) 277–280.
- [43] R. Argazzi, N.Y.M. Iha, H. Zabri, F. Odobel, C.A. Bignozzi, Design of molecular dyes for application in photoelectrochemical and electrochromic devices based on nanocrystalline metal oxide semiconductors, *Coord. Chem. Rev.* 248 (2004) 1299–1316.
- [44] A.S. Poloa, N.Y.M. Iha, Blue sensitizers for solar cells: natural dyes from calafate and jaboticaba, *Sol. Energy Mater. Sol. Cells* 90 (2006) 1936–1944.
- [45] J.N. Freitas, A.S. Gonçalves, M.-A. De Paoli, J.R. Durrant, A.F. Nogueira, The role of gel electrolyte composition in the kinetics and performance of dye-sensitized solar cells, *Electrochim. Acta* 53 (2008) 7166–7172.
- [46] D.P. Birnie, N.J. Bendzko, <sup>1</sup>H and <sup>13</sup>C NMR observation of the reaction of acetic acid with titanium isopropoxide, *Mater. Chem. Phys.* 59 (1999) 26–35.
- [47] V.G. Kessler, G.I. Spijksma, G.A. Seisenbaeva, S. Hakansson, D.H.A. Blank, H.J.M. Bouwmeester, New insight in the role of modifying ligands in the sol–gel processing of metal alkoxide precursors: a possibility to approach new classes of materials, *J. Sol–Gel Sci. Technol.* 40 (2006) 163–179.

- [48] J. Yu, J.C. Yu, W. Ho, Z. Jiang, Effects of calcination temperature on the photocatalytic activity and photo-induced super-hydrophilicity of mesoporous TiO<sub>2</sub> thin films, *New J. Chem.* 26 (2002) 607–613.
- [49] P.M. Sommeling, B.C. O'regan, R.R. Haswell, H.J.P. Smit, N.J. Bakker, J.J.T. Smits, J.M. Kroon, J.A.M. Van Roosmalen, Influence of a TiCl<sub>4</sub> post-treatment on nanocrystalline TiO<sub>2</sub> films in dye-sensitized solar cells, *J. Phys. Chem. B* 110 (2006) 19191–19197.
- [50] D.L. Wood, J. Tauc, Weak absorption tails in amorphous semiconductors, *Phys. Rev. B* 5 (1972) 3144.
- [51] M. Gratzel, Dye-sensitized solar cells, *J. Photochem. Photobiol. C* 4 (2003) 145–153.
- [52] D. Kuang, C. Klein, S. Ito, J.-E. Moser, R. Humphry-Baker, S.M. Zakeeruddin, M. Grätzel, High molar extinction coefficient ion-coordinating ruthenium sensitizer for efficient and stable mesoscopic dye-sensitized solar cells, *Adv. Funct. Mater.* 17 (2007) 154–160.
- [53] M.I. Asghar, K. Miettunen, J. Halme, P. Vahermaa, M. Toivola, K. Aitola, A.P. Lund, Review of stability for advanced dye solar cells, *Energy Environ. Sci.* 3 (2010) 418–426.
- [54] F. Fabregat-Santiago, J. Bisquert, G. Garcia-Belmonte, G. Boschloo, A. Hagfeldt, Influence of electrolyte in transport and recombination in dye-sensitized solar cells studied by impedance spectroscopy, *Sol. Energy Mater. Sol. Cells* 87 (2005) 117–131.
- [55] F. Fabregat-Santiago, J. Bisquert, E. Palomares, L. Otero, D. Kuang, S.M. Zakeeruddin, M. Grätzel, Correlation between photovoltaic performance and impedance spectroscopy of dye-sensitized solar cells based on ionic liquids, *J. Phys. Chem. C* 111 (2007) 6550–6560.
- [56] B.C. O'regan, J.R. Durrant, P.M. Sommeling, N.J. Bakker, Influence of the TiCl<sub>4</sub> treatment on nanocrystalline TiO<sub>2</sub> films in dye-sensitized solar cells. 2. Charge density, band edge shifts, and quantification of recombination losses at short circuit, *J. Phys. Chem. C* 111 (2007) 14001–14010.